analytical chemistry

pubs.acs.org/ac Article

Photocleavable DNA Nanotube-Based Dual-Amplified Resonance Rayleigh Scattering System for MicroRNA Detection Incorporating Molecular Computing-Cascaded Keypad Lock Functionality

Yan Lei Li, Xue Hong Min, Ya Jie Fan, Jiang Xue Dong, Dan Wu, Xiang Ren, Hong Min Ma, Zhong Feng Gao,* Qin Wei, Fan Xia, and Huangxian Ju

Cite This: *Anal. Chem.* 2024, 96, 2983−2989 Read Online

ACCESS | Metrics & More | Article Recommendations | Supporting Information

ABSTRACT: Cascade molecular events in complex systems are of vital importance for enhancing molecular diagnosis and information processing. However, the conversion of a cascaded biosensing system into a multilayer encrypted molecular keypad lock remains a significant challenge in the development of molecular logic devices. In this study, we present a photocleavable DNA nanotube-based dual-amplified resonance Rayleigh scattering (RRS) system for detecting microRNA-126 (miR-126). The cascading dual-amplification biosensing system provides a multilayer-encrypted prototype with the functionality of a molecular computing cascade keypad lock. RRS signals were greatly amplified by using photocleavable DNA nanotubes and enzyme-assisted strand displacement amplification (SDA). In the presence of miR-126, enzyme-assisted SDA produced numerous identical nucleotide fragments as the target, which were then specifically attached to magnetic beads through the DNA nanotube by using a Y-shaped DNA scaffold. Upon ultraviolet irradiation, the DNA nanotube was released into the solution, resulting in an increase in the intensity of the RRS signal. This strategy demonstrated a low limit of detection (0.16 fM) and a wide dynamic range (1 fM to 1 nM) for miR-126. Impressively, the enzyme-assisted SDA offers a molecular computing model for generating the target pool, which serves as the input element for unlocking the system. By cascading the molecular computing process, we successfully constructed a molecular keypad lock with a multilevel authentication technique. The proposed system holds great potential for applications in molecular diagnosis and information security, indicating significant value in integrating molecular circuits for intelligent sensing.

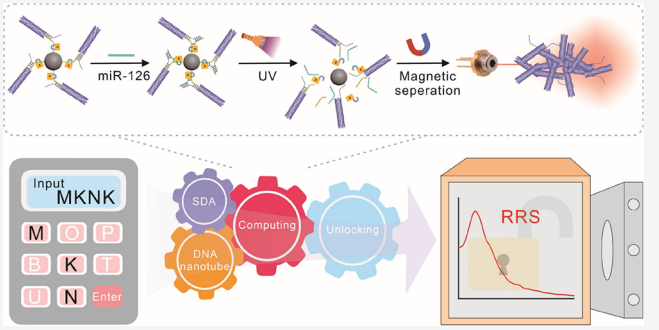

INTRODUCTION

Recently, various logic devices have been created to serve as building blocks for the development of nonsilicon molecular computers.[1−3] These devices utilize biomolecules or chemicals as molecular processors to carry out Boolean operations and handle various inputs, such as nucleic acids, enzymes, light, ions, and organic molecules, to make intelligent output decisions.[4,5] Benefiting from their ability to respond to multiple stimuli, molecular logic operations have shown significant progress in selective analyte sensing and drug delivery.[6−9] One notable logic device is the molecular keypad lock, which only produces output signals when the correct inputs are provided. This lock requires a valid password to be unlocked, allowing for molecular-level data encryption. Consequently, molecular keypad locks have attracted significant attention in the field of information security. Building upon the groundbreaking work of Shanzer and his colleagues in 2007,[10] a wide range of molecular keypad locks have been developed to convert input combinations of nucleic acids, antibodies, enzymes, metals, or gases into electrochemical, colorimetric, or fluorescence outputs.[11−19] However, the lack of effective multilayer strategies for integrating molecular events in complex systems poses limitations to such endeavors. Thus, creating a multilevel encrypted molecular keypad lock by cascading molecular logic computing systems becomes an exceptionally challenging task.

Molecular sensing systems often integrate biomolecules (nucleic acids, enzymes, and peptides) with nanomaterials (metal−organic framework, quantum dots, graphene, noble metal nanoparticles, and nanoclusters) to regulate the sensing interface for biosensing, bioimaging, and logic gate operations.[20−24] The use of expensive labeled biomolecules, such as fluorophores and electrochemically active molecules, restricts the signal capacity and reduces bioaffinity.[25−27] Label-free sensing systems with various output signals, including

Received: October 19, 2023
Revised: January 18, 2024
Accepted: January 22, 2024
Published: February 7, 2024

https://doi.org/10.1021/acs.analchem.3c04718
Anal. Chem. 2024, 96, 2983−2989

Scheme 1. Design Principle of the UV Light-Controlled Dual-Amplification Strategy for Detecting miR-126 by the RRS Method

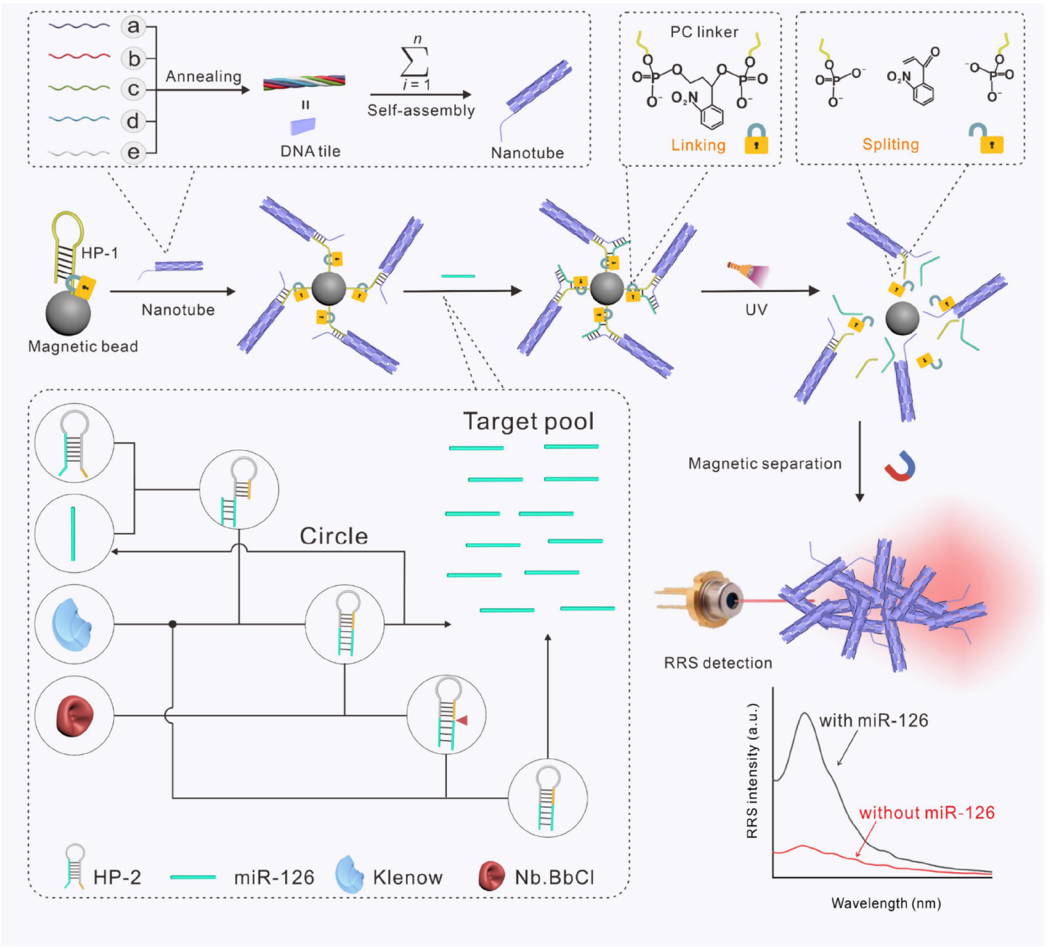

electrochemistry, fluorescence, colorimetry, and so forth, hold significant potential to overcome these limitations.[28−30] Resonace Rayleigh scattering (RRS), which occurs when the wavelength of Rayleigh scattering aligns with or is near the molecular absorption band, has gained significant attention due to its notable selectivity and sensitivity.[31−33] Nonetheless, RRS sensing systems have primarily been utilized solely for detection purposes. The use of RRS sensing systems in intelligent molecular circuits, particularly in molecular keypad locks, has not yet received adequate consideration.

This study reports a highly sensitive RRS system for miR-126 detection and molecular keypad lock using a photocleavable dual-amplification based on DNA nanotubes. The system incorporates a photocleavable unit and enzyme-assisted strand displacement amplification (SDA) to trigger strong RRS signals from DNA nanotubes. Furthermore, the system employs a molecular computation technique to amplify and process these signals, thereby improving the accuracy and reliability of detection. Interestingly, the system includes a keyboard lock function to ensure signal encryption and decryption, thus safeguarding the privacy and security of the detection results. This innovative system has broad potential applications in biomedical research and the information security fields. It provides precise evidence for disease diagnosis and protects data security, thereby minimizing the risk of information leakage.

EXPERIMENTAL SECTION

DNA Nanotube Assembly. First, a mixture of DNA single strands (Table S1, a−e, 2.5 μL, 100 μM) was prepared by adding it to 37.5 μL of 1 × tris acetate-ethylenediaminetetraacetic acid (TAE, 40 mM tris-acetate, 1 mM ethylenediaminetetraacetic acid, pH 7.4) buffer solution. This resulted in a final concentration of 5 μM within a total volume of 50 μL. Subsequently, the formation of nanotubes was achieved through annealing, which involved heating the mixture to 90 °C and gradually cooling it to 25 °C over a period of 6 h by using a polymerase chain reaction (PCR) instrument.

Polyacrylamide Gel Electrophoresis. The experiment involved the combination of five samples of DNA single strands and DNA nanotubes with the loading buffer in a ratio of 5:1. These mixtures were then transferred to newly prepared polyacrylamide gels with a concentration of 12%. Electrophoresis experiments were conducted using a 1× tris borate-ethylenediaminetetraacetic acid (TBE, 89 mM tris-borate, 2 mM ethylenediaminetetraacetic acid, pH 7.4) buffer at a voltage of 90 V for a duration of 1 h. Following the electrophoresis procedure, the DNA bands were subjected to imaging and subsequent analysis through utilization of the gel imaging systems. This was completed after the application of the 4SGelRed nucleic acid dye and allowing for a 10 min staining period, resulting in the acquisition of electrophoresis outcomes.

https://doi.org/10.1021/acs.analchem.3c04718
Anal. Chem. 2024, 96, 2983−2989

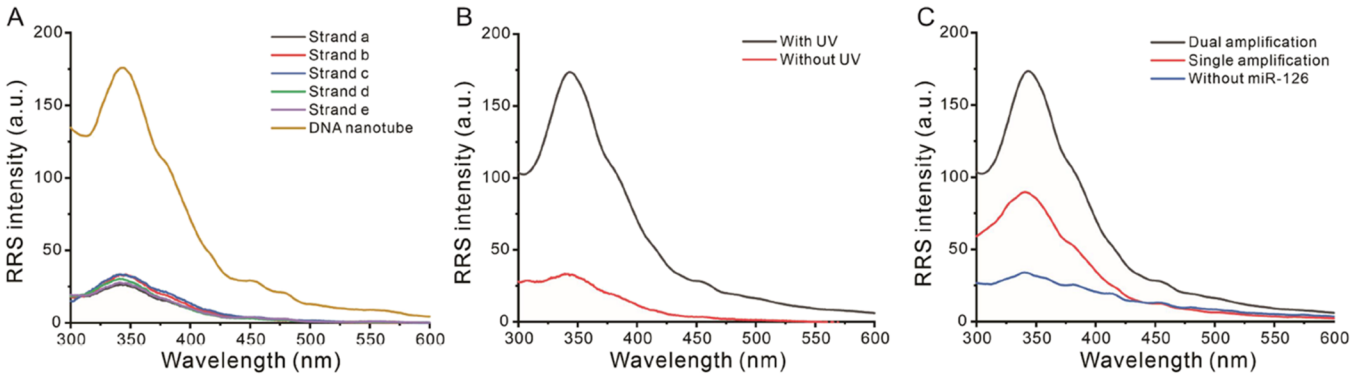

Figure 1. (A) RRS spectra of single-stranded DNA and DNA nanotube. (B) RRS spectra for detecting 1 nM miR-126 with and without UV irradiation. (C) RRS spectra for detecting 1 nM miR-126 using different amplification strategies.

Reaction Procedure for Detecting miR-126. In the process of using DNA hairpin conversion for strand exchange amplification, different concentrations of miRNA are mixed with HP-2 probe (1 μM), Klenow fragment (2 U/mL), dNTPs (2.5 mM), and 10 × NEB 2.1 buffer. The mixture is then treated with Nb.BbvCI at 37 °C for 20 min, followed by the addition of 3 μL of Nb.BbvCI and incubation for 2 h. Afterward, the enzyme is inactivated by heating at 80 °C for 20 min. Next, the biotin-labeled HP-1 probe is bound to the magnetic beads, and the residual nucleic acid chains are removed through washing steps. The Y-shaped DNA structure is dispersed in a Tris-HCl buffer. Finally, ultraviolet (UV) irradiation is used to break the PC-linker connection site, causing the Y-shaped DNA structure to detach from the magnetic beads.

RESULTS AND DISCUSSION

Principle for miR-126 Detection. The design principle of the UV light-responsive DNA nanotube-based RRS biosensor for miR-126 detection is depicted in Scheme 1. First, a hairpin-structured probe, HP-1, is attached to a magnetic bead (MB) using biotin−streptavidin chemistry. This probe has regions that specifically recognize DNA nanotubes and miR-126. At the root of the HP-1 probe, a photocleavable o-nitrobenzyl linker (PC linker) is designed, which only undergoes dissociation upon exposure to ultraviolet light and often serves as a temporary regulator of the probe activity.[34] Five single-stranded DNA (ssDNA, a-e) probes are then combined to form double-crossover DNA tiles, which self-assemble into a DNA nanotube. Next, an efficient SDA strategy is devised to amplify the miR-126 sequences. Another hairpin-structured probe, HP-2, is constructed to integrate the template and primer sequences for SDA into one. This integration enhances the reaction efficiency compared to conventional SDA with a separate template and primer design.[35] A short single-stranded segment acts as a toehold for binding to the miR-126 sequence. After specific recognition, the loop of HP-2 is opened, allowing the single-stranded segment to hybridize with a part of the original loop domain and form another hairpin structure. Additionally, this segment serves as the primer for extension catalyzed by the Klenow fragment polymerase, leading to the release and recycle of the miR-126 sequence. The stem section of the newly formed hairpin contains a restriction site for a nicking endonuclease. By introducing Nb.BbvCI, a nick domain is produced, initiating multiple rounds of polymerization and strand displacement. The resulting mass of single-stranded DNA probes, which serves as the target pool, contains the miR-126 sequence. These DNA probes hybridize with HP-1 and the DNA nanotube to form a Y-shaped DNA scaffold. Due to the large size effect of the released DNA nanotube, it can generate a strong RRS signal after UV irradiation. Without miR-126, the three-arm junction cannot be generated, and the solution does not contain the DNA nanotube after UV irradiation, resulting in a weak RRS signal. By inducing the generation of a three-arm junction through targets and controlling the release of DNA nanotube using UV light, high-sensitivity detection of miR-126 can be effectively achieved.

Self-Assembly and Characterization of DNA Nanotubes. Five individual DNA strands were utilized for the purpose of self-assembling DNA nanotubes and were meticulously examined in accordance with the previous report.[36] As shown in Figure S1, after UV irradiation, the captured DNA nanotube is released into the solution as a result of splitting of the PC linker, which leads to a significant increase in the RRS signal. Figure S2 illustrates the imaging analysis of DNA samples through the utilization of polyacrylamide gel electrophoresis (PAGE). In lanes 1−5, distinct bands denoted as a−e are observed, each exhibiting different migration patterns. Following the self-assembly process, where the five single-stranded DNA probes (a−e) combine to form DNA nanotubes, a prominent band with the highest molecular weight emerges in lane 6, which indicates the successful formation of DNA nanotubes. Moreover, the examination of the DNA nanotube structure was extended by using atomic force microscopy (AFM, Figure S3) and transmission electron microscopy (TEM, Figure S4). As expected, the DNA nanotubes exhibited cylindrical structural features, indicating the successful preparation of DNA nanotubes, and the height of the DNA nanotubes could be clearly observed to reach 1.5 nm.

Analysis of RRS Sensing Platforms. *Validation of the Formation of DNA Nanotube.* To verify the successful growth of the DNA nanotube, the RRS intensity of each individual ssDNA was measured. Figures 1A and S5 illustrate that the RRS intensity of ssDNA only showed a slight increase compared with the buffer sample. This could be attributed to the small size of ssDNA, which does not greatly contribute to light scattering. Nonetheless, a notable increase in RRS intensity was observed when all varieties of ssDNA (a−e) were present, indicating the successful growth of the DNA nanotube in this particular scenario.

https://doi.org/10.1021/acs.analchem.3c04718
Anal. Chem. 2024, 96, 2983−2989

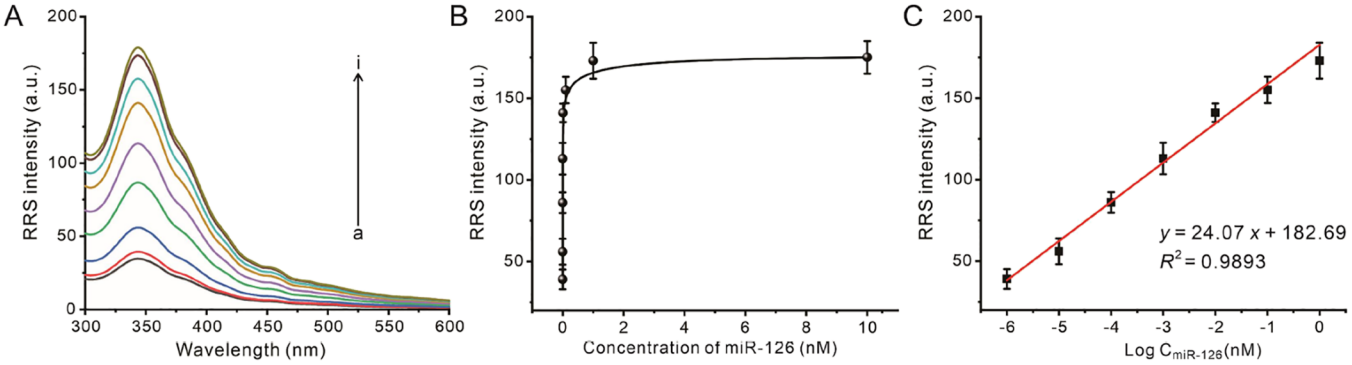

Figure 2. (A) RRS spectra of different concentrations of miR-126. From a to i: 0, 1 fM, 10 fM, 100 fM, 1 pM, 10 pM, 100 pM, 1 nM, and 10 nM. (B) Positive correlation curve between the RRS intensity and the concentration of miR-126. (C) Linear calibration plot of RRS intensity and miR-126 concentration.

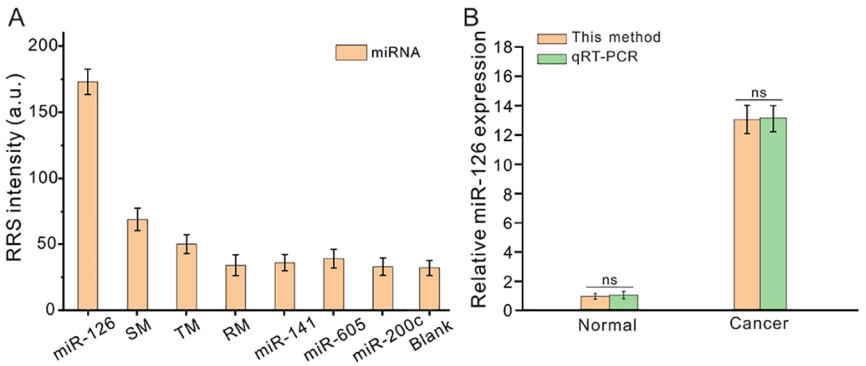

Figure 3. (A) Selectivity test under different substance interference (SM, TM, RM, miR-141, miR-605, miR-200c, and blank). (B) Detection of the relative expression levels of miR-126 (normalized to colonic epithelial cell extracts) between healthy cells and cancer cell extracts by qRT-PCR and the proposed method. Error bars indicate the standard deviation of the three replicates. "ns" means it is not significant at the p = 0.05 level.

Validation of the Photocleavable Behavior. To verify the photocleavable behavior, UV irradiation was selectively used. As shown in Figure 1B, the RRS intensity barely increased without UV irradiation. This phenomenon occurs because DNA nanotubes cannot be released into the supernatant from MB. Conversely, in the presence of UV light, the RRS intensity increased significantly due to the successful release of DNA nanotubes after PC linker splitting. Consequently, UV irradiation proves to be an effective approach for remotely controlling the release of the DNA nanotube.

Validation of the miR-126 Detection. To assess the feasibility of dual-amplification for miR-126 detection, the RRS spectra of different samples were recorded. As shown in Figure 1C, in the absence of miR-126, the activity of DNA SDA was suppressed, preventing the DNA nanotube from binding to the MB. As a result, a low RRS intensity was observed, similar to that of the buffer solution. Without the SDA reaction, the RRS intensity increased 2.73-fold in the presence of 1 nM miR-126 through single amplification using the DNA nanotube. Notably, the RRS intensity was significantly enhanced by 5.24-fold when using the dual-amplification of DNA SDA and the nanotube in the presence of 1 nM miR-126. These results indicate that the proposed sensing system was successfully created.

Optimization of Experimental Conditions. To achieve the best sensing performance of the proposed platform, various experimental conditions were optimized. The self-assembly time of the Y-shaped DNA scaffold was investigated, as depicted in Figure S6. It was observed that the RRS intensity gradually increased over time, reaching a maximum and stabilizing at 60 min. Therefore, the optimal assembly time for the Y-shaped DNA was determined to be 60 min. Another optimization factor was the concentration of enzymes, such as Klenow and Nb.BbvCI. As shown in Figure S7, the RRS intensity reached its peak when the concentration of Klenow was 2 U/mL. Figure S8 displays that the optimal concentration for Nb.BbvCI was 2 U/mL. The duration of UV irradiation is crucial for releasing the DNA nanotube. Figure S9 revealed that the RRS intensity increased as the UV irradiation time increased. After 10 min of irradiation, the RRS intensity reached a plateau.

RRS Response of the Sensing Platform to miR-126. By recording the corresponding RRS spectra, we have examined the quantitative performance of miR-126 under these optimized conditions. As depicted in Figure 2, the RRS intensity progressively increased as the miRNA concentration ranged from 1 fM to 10 nM. Simultaneously, there was a linear correlation between the logarithm of miRNA concentration and the RRS intensity within this detection range. The linear equation derived was I = 24.07 log C + 182.69 (where I represents RRS intensity and C denotes miRNA concentration), exhibiting a correlation coefficient of 0.9893 and a detection limit of 0.16 fM (S/N = 3). Additionally, we compared the sensing performances of the proposed strategy with the recently reported miRNA assays. The results presented in Table S2 demonstrate that this work exhibits a significantly superior sensitivity and a relatively wide linear

https://doi.org/10.1021/acs.analchem.3c04718
Anal. Chem. 2024, 96, 2983−2989

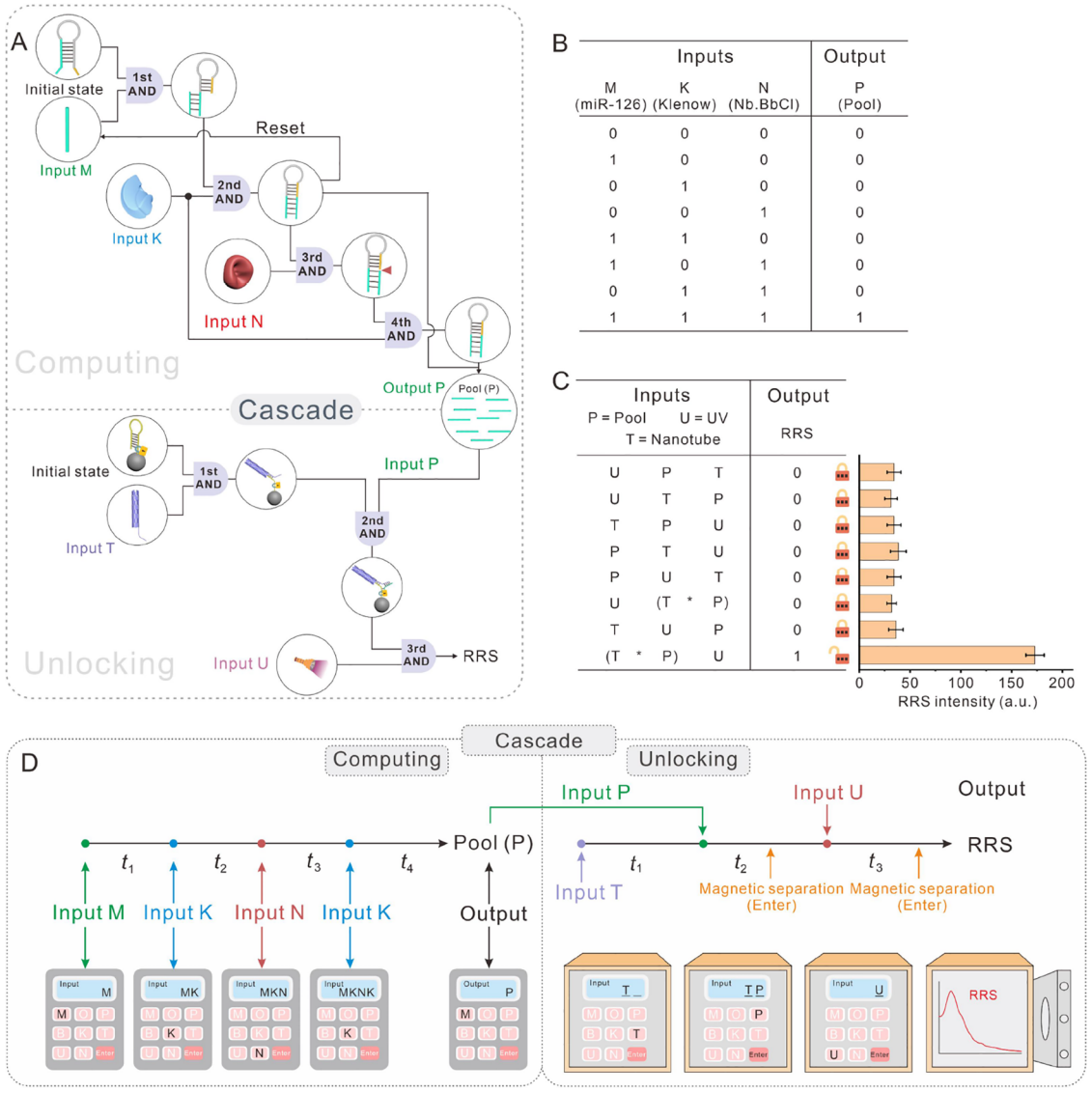

Figure 4. (A) Schematic representation of the RRS sensing system for the cascade logic operating as a molecular keypad lock. Truth table for the (B) molecular computing and (C) keypad lock system. (D) Cartoon representations of miRNA detection incorporating molecular computing-cascaded keypad lock functionality.

range. Therefore, this method holds significant potential for the sensitive detection of miR-126.

Investigation of Selectivity and Practicability. The selectivity of the proposed strategy is explored by comparing single-base mismatched (SM), three-base mismatched (TM), random mismatched (RM) sequences, and various other miRNAs. Figure 3A illustrates that the presence of pure interfering miRNAs does not cause a significant alteration in the RRS intensity. However, upon the addition of miR-126, the peak increases to a level comparable to that of pure miR-126. These findings validate that the proposed sensing strategy can be used for high selective detection of miR-126.

To evaluate the practicality of the proposed sensing strategy in real biological samples, recovery experiments were conducted by introducing varying concentrations of miR-126 to mouse serum samples that were diluted 100 times. As shown in Table S3, the results indicated that the recoveries varied from 96.4 to 106.0% and that the relative standard deviation (RSD) for all tests was below 5%. This demonstrates that the designed biosensor has the potential to be used for detecting miRNA in real samples. Furthermore, the quantitative real-time polymerase chain reaction (qRT-PCR) method was used to determine the expression level of miR-126 in both colonic epithelial and cancerous cells. Figure 3B demonstrates that miR-126 is upregulated in cancerous cells in comparison to normal cells, which aligns with the results of previous studies.[37] Additionally, there were no noteworthy disparities in the measurement of the relative expression levels of miR-126 between the two techniques, verifying the accuracy of the proposed biosensing system.

Molecular Computing-Cascaded Keypad Lock. In the development of molecular computing-cascaded keypad lock systems, designing processing systems for simulating sequential logic operations becomes a challenging step because these operations depend on the combination and sequence of inputs. By applying sequential logic operations, unlocking elements such as molecular triggers, latches, and registers can be constructed. The molecular computing-cascaded keypad lock system we proposed offers higher security and reliability compared with traditional keypad lock systems. The system

https://doi.org/10.1021/acs.analchem.3c04718
Anal. Chem. 2024, 96, 2983−2989

utilizes advanced molecular recognition technology to create a secure lock mechanism through the interaction with specific molecules. This technology provides a higher level of security, as it is difficult to duplicate or bypass without proper authorization. On the other hand, compared to traditional keypad locks, it is less prone to mechanical failures or wear and tear. Traditional keypad locks may have physical buttons that degrade over time. The molecular computing cascade keypad lock system provides additional flexibility in access control. It can offer customizable access permissions, allowing specific individuals to have different access levels based on their authorization. This is particularly useful in multiuser or restricted access environments. Traditional keypad locks typically have fixed codes shared among users, limiting the customization of access privileges. The proposed RRS sensor system enables sequential logic operations by coupling molecular computing with the unlocking process (Figure 4A).

In the field of molecular computing, the enzyme-assisted SDA reaction is specifically designed to produce the target pool, which is defined as Output P. The initial component used is hairpin DNA, which is capable of forming a hybrid with miR-126, representing Input M, in order to establish an AND gate. Subsequently, Klenow, representing Input K, and Nb.BbvCI, representing Input N, are introduced to initiate the SDA reaction. This forms an AND gate amplifier by resetting Input M. The initial hairpin DNA can further bind to miR-126 again through the sequential action of typing M, K, N, and K, resulting in the generation of target pool and outputting P. As depicted in Figure S10, we characterized every step of the DNA cascade network using gel electrophoresis and showcased the proper functioning of each gate. In lane 3, the output production was indicated by inputting M in the initial state. Lane 4 presented the second stage with the addition of K, which indicated the successful enzyme-assisted SDA reaction. By the input of N, the hairpin probe exposed a cleavage site, which did not affect the molecular weight. Therefore, lane 5 yielded the same result as lane 4. Thus, only the combination of M, K, N, and K can trigger the computing system to obtain the logical "1" state (Figures 4B and S11). Conversely, when other input combinations are present, a low RRS signal is detected, indicating the failure of the target amplification. Therefore, the correct input sequence of M, K, and N represents the password to obtain the correct output, which served as the input for the cascaded unlocking operation. By inputting nanotube (representing T) and P, the hairpin DNA can be efficiently opened to form a Y-shaped DNA structure, which can be dissociated from the magnetic beads upon UV irradiation, resulting in a high RRS signal and outputting logical "1" state (Figures 4C and S12). To note, the unlocking operation involves magnetic beads, which should conduct magnetic separation after each step. The magnetic separation treatment was defined as typing "Enter" button. Figure 4D illustrates the logic computing-cascaded molecular keypad lock prototype. The logic computing and magnetic separation enhanced the encryption level and prevented them from being easily cracked. The correct input sequence (T*P)U represents the password to open the keyboard lock, and all other input combinations cannot open the keyboard lock. (T*P) represents the process of washing off after both T and P are inputted. The initial state will form a stable Y-shaped DNA scaffold with T*P, making the structure more stable. This avoids the DNA nanotube detaching from the initial state during the washing process, which would result in the lack of T input in the buffer solution and reduce unnecessary outputs.

CONCLUSIONS

In summary, this work demonstrates a photocleavable DNA nanotube-based dual-amplification RRS platform for miRNA detection and molecular keypad lock application. The system utilizes DNA nanotubes and enzyme-assisted SDA to amplify signals. When the target is present, enzyme-assisted SDA produces a significant amount of the same nucleotide fragment as the target, which the DNA nanotube specifically binds onto the MB through a Y-shaped DNA scaffold. Upon UV irradiation, the DNA nanotube is released into the solution, thereby increasing the RRS signal. Additionally, the molecular computing cascade keypad lock functionality enhances the system security by allowing only authorized user access. The proposed molecular keypad lock comes with intrinsic advantages, including: (i) a dual-amplification strategy that enhances sensitivity and offers the potential for developing a molecular keypad lock; (ii) a multilayer encryption in the molecular keypad lock, achieved through the incorporation of molecular computation and magnetic separation processes, to minimize the risk of information leakage; and (iii) the ability of the proposed system to bridge the gap between bioanalysis and bioinformatics, opening up a new perspective for molecular-level information encryption. Therefore, the system holds great potential for biomedical applications and could have a positive impact on cheminformatics and practical use in related fields.

ASSOCIATED CONTENT

Supporting Information

The Supporting Information is available free of charge at https://pubs.acs.org/doi/10.1021/acs.analchem.3c04718.

Materials and instrument; PAGE assays; AFM and TEM images; RRS intensity of each individual DNA samples; conditional selection; oligonucleotide sequences; comparison data; and recovery tests (PDF)

AUTHOR INFORMATION

Corresponding Author

Zhong Feng Gao − *Key Laboratory of Interfacial Reaction & Sensing Analysis in Universities of Shandong, School of Chemistry and Chemical Engineering, University of Jinan, Jinan 250022, P. R. China;* orcid.org/0000-0002-4667-6212; Email: chm_gaozf@ujn.edu.cn

Authors

Yan Lei Li − *Key Laboratory of Interfacial Reaction & Sensing Analysis in Universities of Shandong, School of Chemistry and Chemical Engineering, University of Jinan, Jinan 250022, P. R. China*

Xue Hong Min − *Equine Science Research and Doping Control Center, Wuhan Business University, Wuhan 430056, P. R. China*

Ya Jie Fan − *Key Laboratory of Analytical Science and Technology of Hebei Province, College of Chemistry and Materials Science, Hebei University, Baoding 071002, P. R. China*

Jiang Xue Dong − *Key Laboratory of Analytical Science and Technology of Hebei Province, College of Chemistry and Materials Science, Hebei University, Baoding 071002, P. R. China*

https://doi.org/10.1021/acs.analchem.3c04718
Anal. Chem. 2024, 96, 2983−2989

Dan Wu − *Key Laboratory of Interfacial Reaction & Sensing Analysis in Universities of Shandong, School of Chemistry and Chemical Engineering, University of Jinan, Jinan 250022, P. R. China;* orcid.org/0000-0002-8732-5988

Xiang Ren − *Key Laboratory of Interfacial Reaction & Sensing Analysis in Universities of Shandong, School of Chemistry and Chemical Engineering, University of Jinan, Jinan 250022, P. R. China;* orcid.org/0000-0002-4321-4282

Hong Min Ma − *Key Laboratory of Interfacial Reaction & Sensing Analysis in Universities of Shandong, School of Chemistry and Chemical Engineering, University of Jinan, Jinan 250022, P. R. China;* orcid.org/0000-0002-7061-8944

Qin Wei − *Key Laboratory of Interfacial Reaction & Sensing Analysis in Universities of Shandong, School of Chemistry and Chemical Engineering, University of Jinan, Jinan 250022, P. R. China;* orcid.org/0000-0002-3034-8046

Fan Xia − *Engineering Research Center of Nano-Geomaterials of Ministry of Education, Faculty of Materials Science and Chemistry, China University of Geosciences, Wuhan 430074, P. R. China;* orcid.org/0000-0001-7705-4638

Huangxian Ju − *Key Laboratory of Interfacial Reaction & Sensing Analysis in Universities of Shandong, School of Chemistry and Chemical Engineering, University of Jinan, Jinan 250022, P. R. China; State Key Laboratory of Analytical Chemistry for Life Science, Department of Chemistry, Nanjing University, Nanjing 210023, P. R. China;* orcid.org/0000-0002-6741-5302

Complete contact information is available at: https://pubs.acs.org/10.1021/acs.analchem.3c04718

Notes

The authors declare no competing financial interest.

■ ACKNOWLEDGMENTS

This work was supported by the National Key Research and Development Program of China (2018YFE0206900), National Natural Science Foundation of China (22176080, 22090050, and 22274062), the Natural Science Foundation of Shandong Province (ZR2023YQ015), the PhD Research Fund Project of Wuhan Business University (2023KB009), and the Taishan Scholar Project of Shandong Province (ZFG).

■ REFERENCES

(1) Andreasson, J.; Pischel, U. *Chem. Soc. Rev.* **2015**, *44*, 1053−1069.
(2) Hu, Y.; Li, C.; Hu, M.; Zhang, Z.; Fu, R.; Tang, X.; Wu, T. *Small* **2023**, *19*, No. 2300207.
(3) Ma, Z.; Zhang, Y.; Zhang, K.; Deng, H.; Fu, Q. *Nano Materials Science* **2023**, *5*, 265−277.
(4) Piranej, S.; Bazrafshan, A.; Salaita, K. *Nat. Nanotechnol.* **2022**, *17*, 514−523.
(5) Erbas-Cakmak, S.; Kolemen, S.; Sedgwick, A. C.; Gunnlaugsson, T.; James, T. D.; Yoon, J.; Akkaya, E. U. *Chem. Soc. Rev.* **2018**, *47*, 2228−2248.
(6) Wu, L. L.; Huang, J. G.; Pu, K. Y.; James, T. D. *Nat. Rev. Chem.* **2021**, *5*, 406−421.
(7) Li, J. Z.; Dong, L. M.; Zheng, L. L.; Fu, W. L.; Zhang, J. J.; Zhang, L.; Hu, Q. Z.; Chen, P.; Gao, Z. F.; Xia, F. *ACS Appl. Mater. Interfaces* **2022**, *14*, 40447−40459.
(8) Gao, G.; Jiang, Y. W.; Zhan, W. J.; Liu, X. Y.; Tang, R. Q.; Sun, X. B.; Deng, Y.; Xu, L. L.; Liang, G. L. *J. Am. Chem. Soc.* **2022**, *144*, 11897−11910.
(9) Zheng, L. L.; Li, J. Z.; Wen, M.; Xi, D.; Zhu, Y.; Wei, Q.; Zhang, X. B.; Ke, G.; Xia, F.; Gao, Z. F. *Sci. Adv.* **2023**, *9*, No. eadf5868.
(10) Margulies, D.; Felder, C. E.; Melman, G.; Shanzer, A. *J. Am. Chem. Soc.* **2007**, *129*, 347−354.
(11) Sun, X.; Xia, T.; Xu, L.; Zhan, W.; Liang, G. *Anal. Chem.* **2023**, *95*, 5839−5842.
(12) Jiang, X. J.; Ng, D. K. P. *Angew. Chem., Int. Ed.* **2014**, *53*, 10481−10484.
(13) Chen, J. H.; Zhou, S. G.; Wen, J. L. *Angew. Chem., Int. Ed.* **2015**, *54*, 446−450.
(14) Ha, S. Y. Y.; Ng, D. K. P. *Chem. Commun.* **2020**, *56*, 14601−14604.
(15) Turkoglu, G.; Koygun, G. K.; Zafer Yurt, M. N.; Pirencioglu, S. N.; Erbas-Cakmak, S. *Chem. Sci.* **2021**, *12*, 9754−9758.
(16) Lu, J. Y.; Zhang, X. X.; Huang, W. T.; Zhu, Q. Y.; Ding, X. Z.; Xia, L. Q.; Luo, H. Q.; Li, N. B. *Anal. Chem.* **2017**, *89*, 9734−9741.
(17) Kumar, G. G. V.; Kannan, R. S.; Yang, T. C. K.; Rajesh, J.; Sivaraman, G. *Anal. Methods.* **2019**, *11*, 901−916.
(18) Wei, B.; Sun, X. B.; Yao, D. B.; Li, C. X.; Xiao, S. Y.; Guo, Y. J.; Liang, H. J. *Chem. Commun.* **2020**, *56*, 7427−7430.
(19) Du, Y.; Han, X.; Wang, C.; Li, Y.; Li, B.; Duan, H. *ACS sensors.* **2018**, *3*, 54−58.
(20) Fan, Y. J.; Dong, J. X.; Li, Y. L.; Wang, Z. G.; Chang, Y. Q.; Ren, L. F.; Su, M.; Guan, L.; Shen, S. G.; Gao, Z. F.; Xia, F. *Anal. Chem.* **2023**, *95*, 11113−11123.
(21) Nannuri, S. H.; Pandey, A.; Kulkarni, S.; Deshmukh, P. K.; George, S. D.; Mutalik, S. *Mater. Today Commun.* **2023**, *35*, No. 106340.
(22) Zhao, S.; Yu, L.; Yang, S.; Tang, X.; Chang, K.; Chen, M. *Nanoscale Horiz.* **2021**, *6*, 298−310.
(23) Campbell, E.; Hasan, M. T.; Gonzalez-Rodriguez, R.; Truly, T.; Lee, B. H.; Green, K. N.; Akkaraju, G.; Naumov, A. V. *Nanomed-Nanotechnol.* **2021**, *37*, No. 102408.
(24) Biscaglia, F.; Ripani, G.; Rajendran, S.; Benna, C.; Mocellin, S.; Bocchinfuso, G.; Meneghetti, M.; Palleschi, A.; Gobbo, M. *ACS Appl. Energy Mater.* **2019**, *2*, 6436−6444.
(25) Zhou, Y.; Ma, W.; Sun, R.; Liu, B.; Zhang, X.; Yang, H. *Biosens. Bioelectron.* **2022**, *214*, No. 114549.
(26) Zhang, X.; Ge, Y.; Liu, M.; Pei, Y.; He, P.; Song, W.; Zhang, S. *Anal. Chem.* **2022**, *94*, 7823−7832.
(27) Liu, M.; Ma, W.; Zhou, Y.; Liu, B.; Zhang, X.; Zhang, S. *ACS sensors* **2023**, *8*, 1867−1867.
(28) Sezemsky, P.; Burnat, D.; Kratochvil, J.; Wulff, H.; Kruth, A.; Lechowicz, K.; Janik, M.; Bogdanowicz, R.; Cada, M.; Hubicka, Z.; Niedziałkowski, P.; Białobrzeska, W.; Stranak, V.; Šmietana, M. *Sens. Actuators B Chem.* **2021**, *343*, No. 130173.
(29) Wang, J.; Pinkse, P. W.; Segerink, L. I.; Eijkel, J. C. *ACS Nano* **2021**, *15*, 9299−9327.
(30) Zhang, F.; Liu, J. *Analysis Sensing* **2021**, *1*, 30−43.
(31) Gao, Z. F.; Zheng, L. L.; Dong, L. M.; Li, J. Z.; Shen, Y.; Chen, P.; Xia, F. *Anal. Chem.* **2022**, *94*, 6371−6379.
(32) El-Kurdi, R.; Patra, D. *Microchim. Acta* **2019**, *186*, 667.
(33) Li, C.; Lin, L.; Bai, H.; Jiang, Z. *Microchem. J.* **2022**, *181*, No. 107760.
(34) Zhang, J. J.; Nie, C.; Fu, W. L.; Cheng, F. L.; Chen, P.; Gao, Z. F.; Wu, Y.; Shen, Y. *Anal. Chem.* **2022**, *94*, 16796−16802.
(35) Miao, P.; Chai, H.; Tang, Y. *ACS Nano* **2022**, *16*, 4726−4733.
(36) Kong, L.; Han, Z.; Zhao, M.; Zhang, X.; Zhuo, Y.; Chai, Y.; Li, Z.; Yuan, R. *Anal. Chem.* **2022**, *94*, 11416−11424.
(37) Phan, N. N.; Moreno, C. S.; Lai, Y. H. *Cytotechnology* **2020**, *72*, 527−537.